Effects of covalency on the *p*-shell photoemission of transition metals: MnO

Paul S. Bagus[1] and Eugene S. Ilton[2]
[1]*Department of Chemistry, University of North Texas, Denton, Texas 76203-5070, USA*
[2]*Pacific Northwest National Laboratory, 902 Battelle Boulevard, P.O. Box 999, Richland, Washington 99352, USA*
(Received 26 September 2005; published 13 April 2006)

The effect of the solid-state environment for an Mn cation in MnO on the Mn $2p$- and $3p$-shell x-ray photoemission spectra (XPS) has been investigated using *ab initio* relativistic wave functions for an embedded MnO_6 cluster model of MnO. These wave functions include many-body effects due to the angular momentum coupling and recoupling of the open-shell electrons. They also include the covalent mixing of the metal d orbitals with ligand p orbitals. The treatment of covalency has not been included previously in *ab initio* theoretical studies of the $2p$-shell XPS of transition-metal complexes. In this work, covalent interactions between the metal and ligands are treated on an equal footing with spin-orbit splittings. The four-component spinors used in these wave functions are optimized separately for the ground and for the $2p$- and $3p$-hole configurations. This orbital relaxation leads to a "closed-shell" interatomic screening of the Mn core hole. The different orbital sets optimized for the ground and core-ionized configurations mean that mutually nonorthogonal orbital sets are used to determine the matrix elements for the XPS relative intensities. Our treatment of the transition intensities is rigorous, and no approximations are introduced to handle the orbital nonorthogonality. The closed-shell screening is important because changes in the XPS obtained for the MnO_6 cluster from that obtained for an isolated Mn^{2+} cation can be directly linked to this screening and to the consequent reduction in the values of certain exchange integrals. The present work is compared to prior, semiempirical calculations; these comparisons allow us to identify unresolved questions about the origin of certain features of the MnO XPS and to suggest further calculations to resolve these questions.

DOI: 10.1103/PhysRevB.73.155110 PACS number(s): 79.60.−i, 82.80.Pv

I. INTRODUCTION

The identification and separation of contributions to the x-ray photoemission spectroscopy (XPS) of transition-metal (TM) cations in ionic materials is a subject of considerable controversy.[1–12] A principal concern has been the importance of interatomic as compared to intra-atomic effects. In order to treat many-body intra-atomic effects with reasonable accuracy, it is necessary that the wave function (WF) include the configuration mixing of nearly degenerate (ND) XPS-forbidden configurations with the XPS-allowed configurations. For $3s$ holes of first-row transition-metal cations, the important ND configurations can often be described as frustrated Auger configurations (FAC's).[13] For p-shell holes, angular momentum coupling and recoupling are the important many-body effects that lead to mixing of recoupled, XPS-forbidden, configurations with the XPS-allowed multiplet-split, angular-momentum-coupled configurations.[1,14–16] Of course, for ionization of shells with nonzero angular momentum $p,d,\ldots$, it is also necessary to take into account the spin-orbit splitting of the shell.[1,3,4,6,15,16] For interatomic many-body effects, the primary focus has been based on the mixing into the WF's of the XPS-forbidden configurations that involve ligand to metal charge transfer. The charge transfer (CT) is considered to be from the highest p level of the closed-shell anionic ligand—i.e., O($2p$) or Cl($3p$)—into the unfilled d shell of the metal,[4,6–9,17] described with the notation $d^{n+1}\underline{L}$; higher-order charge transfers may also be included.[4,6] However, it is known that there are other interatomic effects; these include the crystal-field splitting of the transition-metal d shell[18] and the covalent bonding and mixing of the TM d shell with the ligand p shell orbitals.[2] The book by Cox[19] on the electronic structure of transition-metal oxides provides an excellent general introduction to and review of the importance of covalent interactions in these materials; see, in particular, Chap. 2.2. While Cox and most other work on these oxides are concerned with covalency in the ground state, we have extended this treatment to consider also the mixing of the TM d-shell with the ligand p-shell orbitals in the final, core-ionized, states. In particular, we shall show that this mixing, which is different for initial, unionized, states and for final, core-ionized, states, leads to a screening of the core hole without any change in the formal occupation of the dominantly TM d open-shell orbitals.[2] This is quite different from the CT screening described above that involves adding new configurations of the form $d^{n+1}\underline{L}$ where the number of electrons in the partially occupied, dominantly metal cation d shells is changed. We describe the screening that occurs as a result of the increase in the covalent character of the Mn and O orbitals as closed-shell screening; this clearly distinguishes it from the screening that involves $d^{n+1}\underline{L}$ CT configurations. We show below that closed-shell screening has a direct physical consequence for separation of the peaks in the Mn $2p$ and $3p$ XPS spectra. It is worth noting that the semiempirical, model Hamiltonian formalisms used to calculate the XPS of ionic materials[4,6,18,20] do not explicitly include covalency in the cluster orbitals; rather, it is assumed that the orbitals are either pure metal cation or pure ligand. For MnO and other Mn^{2+} ionic compounds, there is strong evidence and general agreement that CT configurations make, at most, a small contribution to the XPS spectra.[1,5,10,17,21] This minor role of CT configurations makes the theoretical study of MnO ideal to examine the impor-

tance of other interatomic effects for the XPS spectra. In this paper, we report a study of these effects by comparing the results obtained with *ab initio* WF's for an isolated Mn^{2+} cation and for an embedded MnO_6 cluster model of MnO with each other and with experiment.

Essentially all theoretical treatments of many-body effects in the XPS of TM ionic materials use the conceptual framework of configuration interaction (CI) in order to take into account the mixing of XPS-allowed with XPS-forbidden configurations. This is true both for *ab initio* approaches as well as for parametrized semiempirical approaches. For studies that do not depend on parameters adjusted to experiment see, for example, Refs. 1–3, 7–9, 13–17, and 21; for studies that use adjustable parameters, see, for example Refs. 4–6 and the review by deGroot.[18] Furthermore, most theoretical studies of the XPS of TM ionic materials are based on semiempirical cluster models; see, for example, Refs. 4, 6, and 18. In these calculations, values of atomic integrals for the TM are combined with parameters chosen to represent the interaction of the TM with the ligands to construct an effective CI Hamiltonian. Furthermore, the atomic integrals and the interaction parameters used in the semiempirical calculations are commonly adjusted to improve the agreement of the effective Hamiltonian results with experiment.[5] In contrast, *ab initio* many-body CI WF's are free of parameters adjusted to experiment and limitations of the agreement with XPS experiments obtained with these WF's indicate that key physics is missing from the theoretical model used.[13] Many of the studies that use *ab initio* wave functions are based on atomic models, which, of course, exclude a treatment of interatomic effects. There are a relatively small number of *ab initio* XPS studies of oxides that use an embedded cluster of a central metal cation surrounded by nearest-neighbor oxygen anions as a materials model. The 3*s*-hole XPS of MnO (Ref. 8), NiO (Refs. 7, 9, and 22), and CuO (Ref. 23) have been studied as well as the 3*p*-hole XPS of Cr_2O_3 (Ref. 2). However, all of these studies have used nonrelativistic WF's and spin-orbit splittings have been neglected; hence, the metal 2*p* XPS could not be treated. Here, we report results for the Mn 2*p* and 3*p* XPS obtained with relativistic WF's. Our *ab initio* relativistic CI WF's for the MnO_6 cluster include the many-body effects of angular momentum coupling and recoupling within the *d* shell and between the *d* shell and *np* shell with a core hole.[1–3] The orbitals are variationally optimized separately for the initial and final core-hole configurations. The separate optimizations of the four-component spinors for the hole states are necessary in order to have a compact and efficient description of the final-state orbital relaxation in the presence of the core hole. In particular, we use the reoptimization of the orbitals as a simple and direct measure of interatomic closed-shell screening of the core hole. Indeed, the use of different, nonorthogonal sets of orbitals for the initial and final core-hole states is reasonably common with *ab initio* methods; see, for example, Refs. 1–3 and 22–27. The relative XPS energies E_{rel} of the different core-hole states are obtained directly from relativistic CI calculations. The relative XPS intensities I_{rel} are determined using the sudden approximation[28,29] (SA); the SA is exact in the limit of high photon energies[28] and it is appropriate to use[30] for comparing our theoretical results with the XPS measurements of Ref. 1. We have computed the SA I_{rel} exactly, taking into account the nonorthogonality between the orbital sets used for the initial- and final-state wave functions; as discussed in Sec. II, this is a major computational effort. To the best of our knowledge, SA I_{rel} have not been computed for the 2*p* XPS of TM complexes using separately optimized orbital sets for initial and final states.

This paper is organized as follows. In Sec. II, we discuss theoretical and methodological considerations that include (1) the choice of the embedded cluster model used to represent MnO, (2) the choice of configurations for the orbital optimization, (3) the choice of CI WF's, and (4) the methodology used to calculate the SA I_{rel}. In Sec. III, we describe the covalent interaction and mixing of cation 3*d* and ligand 2*p* orbitals and we show that this mixing is considerably larger for the *np*-hole configurations than for the initial configuration. We also discuss the consequences of this covalency for the magnitudes of the two-electron exchange integrals that contribute significantly as a driving force to the multiplet splitting energies. In Sec. IV, we present our results for the Mn 2*p* and 3*p* XPS in MnO using models of both an isolated Mn^{2+} cation and of an embedded MnO_6 cluster. These results are analyzed in terms of the electronic structure of the MnO_6 cluster model. We also place our results in the context of prior work for the Mn 2*p* and 3*p* XPS, which was based on the use of parametrized models. In this connection, we identify a limitation in the many-electron effects taken into account in the theoretical work of Gupta and Sen.[15,16] This is significant given the wide use of Gupta and Sen's results[15,16] for the interpretation of TM XPS, especially as it may provide information about the oxidation state of the TM cation.[31–39] Based on these various comparisons, we identify open issues for the interpretation of the 2*p* and 3*p* XPS of MnO and we discuss further work that could resolve them. Finally, we summarize our conclusions in Sec. IV.

II. MATERIALS MODEL AND THEORETICAL METHODOLOGY

The materials model that we have used for MnO is an MnO_6 cluster embedded in a point-charge environment; the central Mn and six O atoms and the embedding point charges are placed at lattice sites of the MnO crystal.[40] The values of the embedding point charges are adjusted to reproduce the Madelung potential in the region where there is electron density. The charge on the cluster is 10−, consistent with the nominal ionicities. This MnO_6 cluster model has been used in previous studies.[8,41] Four-component spinor orbitals were optimized separately for the initial, 2*p*-hole, and 3*p*-hole configurations. A shorthand for the initial and final configurations is $3d^5$, $2p^53d^5$, and $3p^53d^5$; this notation neglects covalent mixing of the Mn(3*d*) with O(2*p*) (Refs. 2 and 41) and neglects the ligand-field splitting of the Mn(3*d*). Taking account of the ligand-field splitting in the O_h symmetry of MnO, the ground state is $t_{2g}^3e_g^2$ coupled high spin to $^6A_{1g}$ and the XPS-allowed *np*-hole state configurations are $t_{1u}^5(np^5)t_{2g}^3e_g^2(^6A_{1g})$ where the total coupling is either $^7T_{1u}$ or $^5T_{1u}$.[1,3] Here and generally throughout the paper, we use either the familiar O_h point-group representation or atomic

symmetry notation; however, the relativistic calculations take account of the appropriate relativistic double-group representations.[42] The orbitals were determined as Dirac-Fock self-consistent-field (DF-SCF) solutions for the average of configurations.[43] This average is over all possible angular momentum couplings of the open-shell electrons.[1–3] The Dirac CI (DCI) WF's for the cluster involved the mixing of determinants formed from all possible distributions of the five d electrons into the e_g and t_{2g} orbitals together with, for the p-hole states, all possible distributions of five p electrons into the t_{1u} orbitals. This DCI is described as a complete open-shell CI since all distributions of the open-shell electrons are allowed.[43] The DF-SCF and DCI calculations were performed with the DIRAC program system;[44] the output of DIRAC was coupled to programs that we developed to analyze the WF's and to compute[28,29] the SA I_{rel}. The XPS results for the isolated Mn^{2+} cation, used for comparison with the results for the embedded MnO_6 cluster, are essentially the same as reported previously.[1] We have not used a point-charge field about the cation, as was done in Ref. 1, but this introduced negligible changes. For certain purposes, nonrelativistic WF's were computed for the ground and Mn $2p$- and $3p$-hole configurations of the embedded MnO_6 cluster; for these calculations, the CLIPS program system[45] was used.

When *ab initio* WF's based on variational calculations are used to describe core-excitation processes, it is reasonably standard to use different sets of orbitals for the initial, unexcited, and for the final, core-hole excited states.[1–3,22–27] The use of orbitals optimized for final, core-hole states is particularly important for describing the XPS of ionic materials using embedded cluster models of these materials.[2,22,23] This optimization is necessary in order to have a compact and efficient description of the final-state relaxation, including the interatomic closed-shell screening of the core hole. The calculation[28,29] of the XPS SA I_{rel} involves evaluating many-electron overlap integrals between the initial-state WF where a core-electron has been annihilated and the final-state WF's.[46–48] This overlap integral is expanded as a sum of overlap integrals between the individual Slater determinants used to expand the initial- and final-state DCI WF's. While the calculation of the many-electron overlap integral is not particularly time consuming if the WF's involve only one or a few Slater determinants, it becomes expensive and difficult when the WF's are linear combinations of many determinants. This latter case arises quite often.[49] For the present work, the WF's involved expansions for the initial states of more than 100 determinants and for the final states of ~750 determinants; these are sufficiently large CI's that the calculation of the I_{rel} is not negligible. Furthermore, it was necessary to calculate the SA I_{rel} for a large number of final states and for a few degenerate or nearly degenerate initial states. Thus, the calculation of the many-electron overlap integrals is a major computational burden. A numerically efficient program to compute overlap and other one-electron integrals between CI wave functions expanded in nonorthogonal orbital sets is included in the ALCEHMY program package for the calculation of nonrelativistic WF's.[50] This program is based on the cofactor method for evaluating the integrals between Slater determinants.[47,48] The program, which has been extended to handle the case of relativistic CI wave functions where the Slater determinants are formed with four-component spinors, was used to determine the SA I_{rel}.

III. BONDING AND OTHER PROPERTIES OF THE CLUSTER WAVE FUNCTIONS

Our DCI WF's do not include $d^{n+1}\underline{L}$ configurations to represent CT screening but they do include the closed-shell screening that is obtained by allowing the covalent mixing of Mn $3d$ and the O $2p$ character in filled bonding and half-filled antibonding spin orbitals.[2] Before we turn to the computed Mn p-shell XPS spectra for MnO, we consider the extent of the closed-shell screening by examining several properties of the WF's and indicate how this screening will modify the MnO XPS from that for an isolated Mn^{2+} cation. For the purpose of this analysis, we have used nonrelativistic Hartree-Fock (HF) WF's for the average of configurations for the ground- and np-hole-state configurations. This is because programs to compute the properties of interest are already available for the nonrelativistic WF's. Since our concern is for the overall character of the orbitals and for the way this character changes between an isolated Mn^{2+} cation and Mn in the MnO environment, the use of nonrelativistic HF WF's is satisfactory.

We examine first the amount of Mn $3d$ character in the closed shells of t_{2g} and e_g symmetries and in the half-filled open-shell orbitals of these symmetries. In crystal-field theory,[42] these orbitals are pure ligand and pure TM d shell, respectively; this approximation for the orbitals is also made with semiempirical cluster models of the XPS of ionic TM materials.[4,6,51] In ligand-field theory, the highest-lying closed-shell orbitals, while dominantly of ligand np character, have bonding character with the TM d orbitals and the open-shell orbitals, while dominantly of TM d character, are antibonding with the ligand np orbitals.[41,42] To determine the extent of the d character in these mixed orbitals, we project the atomic d functions from the initial, $3d^5$, configuration of the isolated Mn^{2+} cation onto the orbitals of the MnO_6 cluster.[52] This projection procedure avoids uncertainties associated with the more traditional population analyses.[53] The sensitivity of the projections to the particular choice of atomic $3d$ orbitals was tested and found to be small. The numbers of Mn d electrons in the open shells and the numbers summed over all the occupied shells are given in Table I for the HF WF's for the ground and for the np-hole configurations.

The covalent bonding reduces the number of d electrons in the open shells from the nominal values of $n_d(t_{2g})=3$ and $n_d(e_g)=2$ although these orbitals still have dominantly Mn $3d$ character. The closed-shell bonding, nominally pure ligand, orbitals acquire a modest amount of d character. Indeed, since the occupation of these orbitals is double that of the open-shell orbitals, the gain of d character in the closed shells exceeds the loss in the open shells and there is a net gain of d electrons caused by the covalent bonding of the metal with the O ligands. The changes in n_d due to the covalent interaction in e_g symmetry are larger, typically by factors of ~3, than in t_{2g} symmetry. The chemical reason for the larger covalent interaction in e_g symmetry is clear; the e_g

TABLE I. Projection of the number of $3d$ electrons, n_d, for the ground and p-hole configurations of the embedded MnO_6 cluster. Projections are from the open shell t_{2g} and e_g orbitals and from the sum over all the occupied t_{2g} and e_g orbitals; the row "Total n_d" sums the contributions from the t_{2g} and e_g symmetries. The results are for nonrelativistic WF's.

n_d	$3d^5$	$3p^5 3d^5$	$2p^5 3d^5$
Open shell t_{2g}	2.93	2.87	2.83
Open shell e_g	1.83	1.64	1.56
Total t_{2g}	3.06	3.12	3.11
Total e_g	2.16	2.35	2.40
Total n_d	5.22	5.47	5.51

orbitals are directed toward the O ligands while the t_{2g} orbitals are directed between the ligands.[42] For the ground d^5, or $t_{2g}^3 e_g^2$, configuration, the open-shell t_{2g} orbital has 98% $3d$ character while the open-shell e_g orbital, which loses $\sim$0.16 d electrons, is still 92% Mn $3d$. The e_g and t_{2g} closed shells gain 0.33 and 0.13 $3d$ electrons, respectively. Due to this covalent mixing, the total number of $3d$ electrons in the initial-state configuration increases by only 4% to $n_{3d}=5.22$.

The situation is quite different for the np-hole configurations where n_{3d} increases by 10% over the nominal value of 5. The orbital interactions are similar for the $2p$-hole and $3p$-hole configurations since both $2p$ and $3p$ are core electrons and we will discuss the orbital properties only for the $2p$-hole case. The antibonding open-shell e_g orbital loses 0.44 $3d$ electrons and now has only 78% $3d$ character. Because of the greater $3d$ occupation of the closed e_g shells, the total $n_d(e_g)=2.40$ is increased by 20% over the nominal value of 2. The increase of covalent character for the p-hole orbitals over that for the ground configuration leads to a closed-shell screening of the p hole by $\sim$0.3 electrons. The interatomic screening due to this covalent interaction is significant; however, it is smaller than the closed-shell screening that we found for Cr^{3+} in Cr_2O_3 where, for a $3p$ hole on Cr, the net charge transfer from O to Cr($3d$) was more than twice as large, 0.7 electrons.[2] Further study is required to evaluate the relative importance, for the magnitude of the closed-shell screening, of the charge state of the TM cation and of its position in the row of TM elements. However, at this point, we are able to state that the larger role of covalency when there is a core hole on the TM cation contributes significantly to the screening of the core hole. We stress that this closed-shell screening does not involve $d^{n+1}\underline{L}$ configurations that change the occupation of the open shells associated with the TM cation. The changes in covalent character between the initial and np-hole configuration orbitals clearly demonstrate the need to take the orbital overlaps into account when the SA intensities[46–48] are computed to simulate the XPS spectra.

It is common practice to use contour plots of orbitals and of orbital densities to provide a visualization of the electronic interactions and to provide a graphical way to relate these interactions to materials properties. In particular, these plots may be drawn in a two-dimensional plane where the contours are the lines, in that plane, where the orbitals, or the orbital densities, have a constant value. Such graphical displays have been used to elucidate the electronic interactions for a wide range of physical problems including (1) the analysis of the physisorption of rare gases on metal surfaces,[54] (2) the surface electronic structure of perovskite superconductors,[55] and (3) the properties of amorphous glasses.[56] In the present work, we use contour plots of the higher-lying e_g orbitals, φ, for the ground and $2p$-hole configurations, which are shown in Figs. 1 and 2, respectively. In these plots, solid lines are contours where φ is positive, long-dashed lines are contours where $\varphi<0$, and short-dashed lines are where $\varphi=0$. The plotting plane contains the Mn nucleus at the center and four O nuclei near the corners of the square plot region; the changes in value between adjacent contours is 0.025 $(\text{bohr})^{-3/2}$. For the ground $t_{2g}^3 e_g^2$ configuration, Figs. 1(a) and 1(b) are for the open-shell, $4e_g^2$, and for the highest-lying closed-shell, $3e_g^4$, orbitals, respectively, of the embedded MnO_6 cluster. Figures 2(a) and 2(b) are for the same orbitals but for the configuration with a $2p$ core hole. In both cases, the e_g orbital with d_{xy} character is plotted. The zero between the Mn $3d$ and O $2p$ contributions in Figs. 1(a) and 2(a) shows the antibonding character of this orbital, while the much larger number of d_{xy} than O $2p$ contours

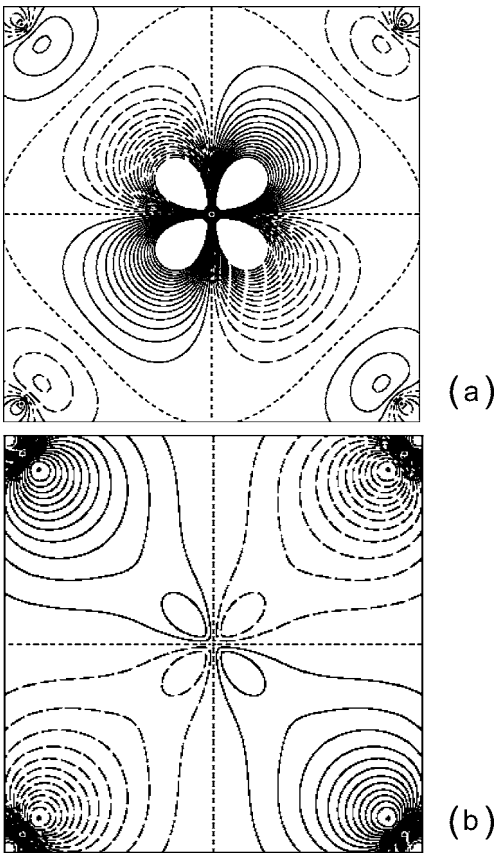

FIG. 1. Contour plot for the $3d^5$ configuration of MnO_6: (a) the open-shell $4e_g^2$ orbital and (b) the closed-shell $3e_g^4$ orbital. The Mn atom is at the center of the plot, and the four O atoms are near the corners of the plot region. The solid contour lines are for positive values of the orbitals, long-dashed lines for negative values, and short-dashed line for zero. The changes in value between adjacent contours is 0.025 $(\text{bohr})^{-3/2}$.

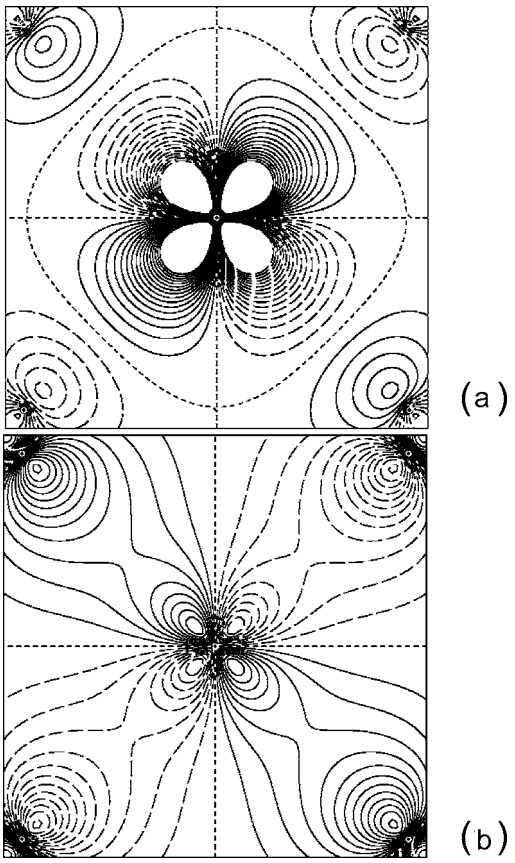

FIG. 2. Contour plot for the $2p^5 3d^5$ configuration of MnO_6: (a) the open-shell $4e_g^2$ orbital and (b) the closed-shell $3e_g^4$ orbital; see caption to Fig. 1.

shows the dominant $3d$ character of these orbitals. The contours joining the O and Mn centers show that the orbitals in Figs. 1(b) and 2(b) are bonding, while the larger number of contours centered on O show the dominant O character of these orbitals. However, comparing Figs. 1(a) and 1(b) with Figs. 2(a) and 2(b) clearly shows the significant increase in covalent character for the orbitals when the $2p$ core hole is present. Further, the closed-shell screening is graphically demonstrated in Fig. 2(b) where there are several contours around the Mn nucleus.

It is appropriate to ask how the modest increase in covalency will affect the XPS spectra. The open-shell ligand-field-split d orbitals retain their dominant d character; this is shown in Table I. Furthermore, the $2p$ and $3p$ core levels retain their atomic identity. Thus the intra-atomic multiplet splitting[1,3,57] and the intra-atomic many-body configuration mixing that describe the angular momentum coupling and recoupling[1,3] should not be qualitatively changed because of the covalent bonding in condensed-phase MnO. However, the delocalization of the contracted atomic Mn $3d$ orbitals that results from the covalent mixing of the ligand $2p$ and metal $3d$ orbitals will reduce the two electron Coulomb, J, and exchange, K, interaction integrals,[57] involving the $3d$ orbitals. The integrals are denoted $J(i,j)$ and $K(i,j)$ for integrals between the ith and jth orbitals.[58,59] In particular, the exchange integrals $K(i,j)$ drive the multiplet-splitting- and the angular-momentum-recoupling many-body effects;[57] thus, if these integrals are reduced, it is to be expected that the energy separations will be reduced by comparable amounts. In order to simplify the comparisons of the exchange integrals for Mn^{2+} with those for MnO_6, we consider average values of K, denoted $\bar{K}$. The integrals of interest are $\bar{K}(3d,3d)$, $\bar{K}(3p,3d)$, and $\bar{K}(2p,3d)$ where the label $n\ell$ is used to denote both atomic and cluster orbitals; the averages are taken over the three p or t_{1u} orbitals and over the five atomic d or the sum of the three t_{2g} and two e_g cluster orbitals. The $\bar{K}(3d,3d)$ will affect primarily the energy separation of different couplings of the d^5 shell while the $\bar{K}(np,3d)$ will affect primarily the energy separation of different couplings between the np and $3d$ shells.[57] The values of these $\bar{K}$ integrals are given in Table II for the HF orbitals for the initial and np-hole configurations of both the isolated atom and the MnO_6 cluster. For the same configuration, the values of $\bar{K}$ for MnO_6 are smaller than for the isolated Mn^{2+} cation. This is exactly as expected because of the covalent character of these orbitals as shown in Table I. For the initial d^5 configuration, the reductions of the MnO_6 $\bar{K}$ over the cation values are small, $\sim 2\% - 3\%$, consistent with the small covalency of the d orbitals for this configuration; see Table I and Fig. 1. The reductions of $\bar{K}$ for the p-hole configurations are significantly larger, ranging between 6% and 10%. It should be noted that it is common practice in semiempirical cluster model calculations to scale the atomic integrals to smaller values.[18] However, the explanation commonly given to justify this scaling is that it takes into account electron correlation effects not included in the model Hamiltonian.[18] We have shown that an important reason for the decrease of the

TABLE II. Average exchange integrals $\bar{K}$ in eV among the $2p$, $3p$, and $3d$ orbitals for the HF WF's for the isolated Mn^{2+} cation and the embedded MnO_6 cluster. Values are given for the initial configuration, $3d^5$, and for the p-hole configurations, $3p^5 3d^5$ and $3p^5 3d^5$. The decrease of the MnO_6 integrals is noted in parentheses.

Configuration	$\bar{K}(3d,3d)$		$\bar{K}(3p,3d)$		$\bar{K}(2p,3d)$	
	Mn^{2+}	MnO_6	Mn^{2+}	MnO_6	Mn^{2+}	MnO_6
$3d^5$	5.44	5.20 (−3.0%)	2.67	2.62 (−1.9%)	0.71	0.70 (−1.7%)
$3p^5 3d^5$	5.93	5.44 (−8.4%)	2.86	2.68 (−6.1%)		
$2p^5 3d^5$	6.31	5.69 (−10.0%)			0.96	0.90 (−6.9%)

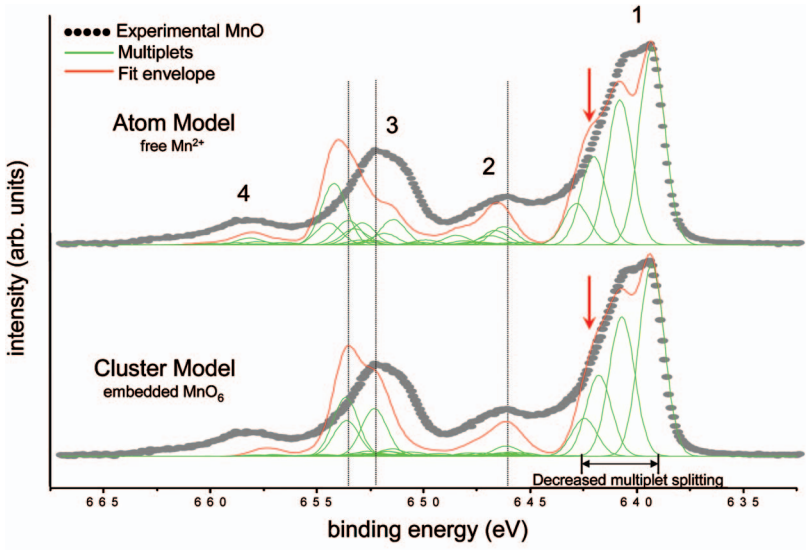

FIG. 3. (Color) $2p$ XPS for Mn^{2+} and for the embedded MnO_6 cluster compared to experiment. For both the atomic and cluster model results, the first calculated multiplet at $E_{rel}=0$ eV has been placed at $E=639.3$ eV to give the best fit to the experimental $2p$ XPS for MnO.

electrostatic integrals arises from the covalent mixing of ligand and TM d orbitals. We also note that when the two electron integrals are correctly computed with orbitals variationally optimized for the hole-state configurations, they are larger than the integrals computed with orbitals optimized for the initial-state configuration. This increase in the integrals occurs both for the isolated cation Mn^{2+}, as well as for the embedded MnO_6 cluster; the data in Table II show that the increases are large, ~10% or even more. The $3d$ electrons see a larger effective charge in the hole-state[17,60] configurations than in the initial-state configurations and, hence, the $3d$ orbitals are more contracted in the hole states, leading to larger electrostatic integrals.[57] This increase of the hole-state two-electron integrals needs to be taken into account, and one should avoid using integrals computed for the initial-state configuration as a basis for computing the metal np XPS as was sometimes done in earlier work.[15,16,20]

IV. XPS SPECTRA OF MnO

The changes introduced into the orbitals when an Mn cation is placed in the environment of MnO have been discussed above. We are now ready to compare the theoretical XPS spectra for the isolated Mn^{2+} cation and for the embedded MnO_6 cluster with experimental spectra. The experiment for MnO is as reported in Ref. 1. The theoretical spectra were obtained using a Gaussian broadening of the theoretical SA intensities.[28,29] to account for lifetime and instrumental broadening;[3] the same broadening of 1 eV was used for all peaks. The position of the first theoretical XPS peak was adjusted to line up with the leading edge of the experimental XPS; no other adjustments were made to the theoretical results.

A. Mn 2p XPS

We consider first the comparisons for the Mn $2p$ XPS, shown in Fig. 3. For the theoretical spectra, the contributions of individual ionic levels from the DCI WF's, or of closely spaced levels, are shown as well as the envelope of the sum of the individual levels. In this figure, we refer our calculated relative energies E_{rel} to the measured XPS energies with an energy scale where $E_{rel}=0$ is placed at 639.3 eV. Four specific regions are highlighted in Fig. 3. These are the first peak from $0 \leqslant E_{rel} \leqslant \sim 3.5$ eV, the second peak at $\sim 6.0 \leqslant E_{rel} \leqslant \sim 9.0$ eV, the third peak at $\sim 11.0 \leqslant E_{rel} \leqslant \sim 16$ eV, and the fourth peak at $\sim 16.0 \leqslant E_{rel} \leqslant \sim 22$ eV. Here, $E_{rel}=0$ for the first calculated level shown in Fig. 3.

The first Mn($2p$) XPS peak contains contributions from four ionic levels. These can best be viewed as the open d shell, $3d^5(^6S)$ coupled to $J=5/2$, coupled with the Mn $2p^3_{3/2}$ hole with $j=3/2$ leading to total J values of 4, 3, 2, and 1; the use of J as a good quantum number is rigorous for Mn^{2+} and approximate for MnO.[42] For this particular peak, the splitting of the J levels due to the reduced degeneracy in the O_h^* double group arising from ligand-field effects is only $\leqslant 0.003$ eV. For this first peak, the use of atomic symmetry is an extremely good approximation. However, the theoretical spectra for MnO_6 is ~0.4 eV, or 10%, narrower than for Mn^{2+}; see the vertical arrows in Fig. 3. This improves the agreement of theory and experiment. In addition, the doublet structure in the theory is reduced for the MnO_6 cluster model of MnO; this brings the theory closer to experiment where there is only a shoulder rather than a distinct second peak in the spectrum. The problem still remains for the MnO_6 cluster that the calculated energies of the $J=3$, $J=2$, and $J=1$ levels are slightly too high relative to the $J=4$ level. However, the overall fit to experiment is considerably improved for the MnO_6 cluster model by the narrowing of the spacing of the levels contained in this first peak. In Table III, a detailed comparison of the E_{rel} and I_{rel} between Mn^{2+} and the MnO_6 cluster is given for this first XPS peak. The E_{rel} for the first, $J=4$, level is set to zero, and the I_{rel} is normalized to 9, or the number of degenerate states in the $J=4$ level. The normalization is chosen to allow a direct identification of the importance of many-body effects for the various levels. In the absence of many-body effects, the SA I_{rel} will scale as the number of degenerate states for a particular level or for a Russell-Saunders multiplet.[61] Thus, with the normalization we have used, the departures of $I_{rel}(J)$ from $2J+1$ indicate

TABLE III. The individual $2p$-hole levels in the first XPS peak for $0 \leqslant E_{rel} \leqslant 3.5$ eV for the Mn^{2+} and MnO_6 cluster models of MnO. For Mn^{2+}, J is a good quantum number, while for MnO_6, it is a good approximation. The E_{rel} for the different levels are in eV. The I_{rel} are normalized to 9 for the first level, which is the degeneracy of this level. For MnO_6, the numbers of $2p_{1/2}$ and $2p_{3/2}$ electrons, $n(2p_{1/2})$ and $n(2p_{3/2})$, in the DCI WF's for the various levels are also given.

		Mn(2+)		MnO_6			
J	Degeneracy	E_{rel}	I_{rel}	E_{rel}	I_{rel}	$n(2p_{1/2})$	$n(2p_{3/2})$
4	9	0	9	0	9	2.00	3.00
3	7	1.51	6.61	1.41	6.53	1.97	3.03
2	5	2.74	4.02	2.49	3.78	1.97	3.03
1	3	3.54	1.88	3.18	1.76	1.99	3.01

that many-body effects are leading to a loss of intensity into satellites. The E_{rel} for the MnO_6 cluster model of MnO are consistently from ~0.1 to ~0.4 eV smaller than for the isolated Mn^{2+} cation. These reductions of ~10% in the E_{rel} are comparable to the decrease of the $\bar{K}(2p,3d)$ exchange integral for the $2p$-hole-state configuration; see Table II. The splitting of the energies of the J levels is a complicated formula involving the $K(2p,3d)$ exchange integrals and the spin-orbit coupling parameters within the $2p$ and $3d$ shells.[15,62] However, in the limit that the d^5 shell is a pure Russell-Saunders multiplet coupled to $^6S_{5/2}$ and the $2p$ hole is a pure $p_{3/2}$, then the splitting of the J levels depends only on the $K(2p,3d)$ exchange integrals. Thus, it is not surprising to see that the main consequence of using the MnO_6 cluster model with reduced exchange integrals is a modest reduction in the width of the first XPS peak in the Mn $2p$ spectra. The I_{rel} in Table III also show that the values for the MnO_6 levels are reduced from those for Mn^{2+} by ~1% for $J=3$ to ~6% for $J=2$ and $J=1$. Thus, many-body configuration mixing, which steals intensity from the allowed configurations into higher-energy "satellites,"[1,3,14–16,63] is somewhat more important for the cluster than for the isolated cation. Larger configuration mixing is expected to lower the energy of the lowest states since the trace must remain invariant. Thus the larger CI mixing for the MnO_6 cluster model of MnO may also contribute to the narrowing of the first peak.

If there were no many-body effects, all the intensity of the $2p_{3/2}$ photoionization would be present in the first XPS peak. Summing the values of I_{rel} for the MnO_6 cluster and dividing by the sum of the degeneracies suggests that 13% of the $2p_{3/2}$ intensity is lost to satellites in the space of the CI considered. Of course, additional intensity is lost to higher-energy shake states[61,64] because the final-state orbitals change their character.[28] A more careful analysis confirms that the $2p_{3/2}$ intensity lost from the first peak to other states in the DCI is 13%; this confirms that the $J=4$ level is dominated by a single term that is $2p_{3/2}^3(^6S_{5/2})$ coupled with $3d^5(^6S_{5/2})$ to form a $J=4$ level. Also included in Table III are the numbers of $2p_{1/2}$ and $2p_{3/2}$ electrons, $n(2p_{1/2})$ and $n(2p_{3/2})$, in the WF's for the various levels. These occupations are obtained by summing the $2p_{1/2}$ and $2p_{3/2}$ occupations for each determinant in the DCI WF weighted by the square of the CI coefficient. For a perfect $2p_{3/2}$ hole, the occupations are $n(2p_{1/2})=2$ and $n(2p_{3/2})=3$; the $n(2p_j)$ given in Table III show that the levels in this first peak are very strongly dominated by $2p_{3/2}$ ionization.

TABLE IV. The decomposition of the SA intensity for the MnO_6 cluster model of MnO into intensity due to $2p_{3/2}$ and $2p_{1/2}$ photoionization, $I_{rel}(2p_{3/2})$ and $I_{rel}(2p_{1/2})$, in each of the four regions of energy, in eV, where there are significant XPS Mn($2p$) peaks. The I_{rel} are also given for the energy regions other than those of the four peaks, labeled "Other energies," and for the total I_{rel} summed over all states included in the DCI.

Peak	Energy	$I_{rel}(2p_{1/2})$	$I_{rel}(2p_{3/2})$
1	$0 \leqslant E_{rel} < 3.5$	0.04	2.67
2	$6.0 \leqslant E_{rel} < 9.0$	0.16	0.20
3	$11.0 \leqslant E_{rel} < 16.0$	1.18	0.09
4	$16.0 \leqslant E_{rel} < 22.0$	0.11	0.01
	Other energies	0.04	0.08
Total		1.54	3.09

In order to understand the way in which the $2p_{3/2}$ and $2p_{1/2}$ intensity is distributed over the four XPS peaks shown in Fig. 3, we give in Table IV, a decomposition of the intensity in each of the four regions where there are major XPS peaks. The decomposition is into intensity due to ionization of a $2p_{3/2}$ electron, $I_{rel}(2p_{3/2})$, and of a $2p_{1/2}$ electron, $I_{rel}(2p_{1/2})$. The normalization for the I_{rel} given in Table IV is such that the intensities of $I_{rel}(2p_{3/2})$ and $I_{rel}(2p_{1/2})$ would be 4 and 2, respectively, if the orbitals for the initial- and final-state WF's were the same. In this idealized case, the total relative intensities of $2p_{3/2}$ and $2p_{1/2}$ simply reflect the occupation of the respective shells. In order to determine the intensities for a given final level, or a closely spaced group of final levels, we sum over degenerate final states and average over degenerate initial states.[61] We then apply a common scaling factor to obtain a suitable normalization for I_{rel}; it needs to be stressed that the intensities for $2p_{1/2}$ and $2p_{3/2}$ cannot be scaled separately but a common factor must be used. In addition to the I_{rel} in the energy regions of the four XPS peaks, we also give, in Table IV, the decomposition of the intensities in the other energy regions and of the intensities summed over all the states included in our complete open-shell space DCI, denoted as "total I_{rel}." For both $2p_{3/2}$ and $2p_{1/2}$, the total I_{rel} are 77% of the ideal values of 4 and 2, respectively. This indicates that 23% of the XPS intensity is lost to so-called "shake" states,[28,29,61,64–66] which are not included in our DCI. While some of these shake states may be in the XPS energy range that we are examining, we expect the large majority to be at high energies and outside the energy range of interest in this work.[64,66] In a one-electron model, all the $2p_{3/2}$ intensity would be in the levels of the first peak, $0=E<3.5$ eV; the data in Table IV show that only 87% of the total $I_{rel}(2p_{3/2})$ is in this first peak and 13% is lost by many-electron effects to levels in other energy regions. Table IV also confirms the small contribution of $I_{rel}(2p_{1/2})$, ~1.5%, to the intensity of this peak. Peak 3, $11 \leqslant E_{rel}$

<16 eV, contains most of the $2p_{1/2}$ XPS intensity and very little SA intensity due to $2p_{3/2}$; $I_{\mathrm{rel}}(2p_{3/2})$ is only 8% of the intensity in this peak. However, 24% of the total $I_{\mathrm{rel}}(2p_{1/2})$ is lost by many-electron effects to other energy regions; this loss is almost twice the loss of the $2p_{3/2}$ intensity from peak 1. Figure 3 shows that two sets of levels, at $E_{\mathrm{rel}}\sim 13.0$ eV and ~ 14.4 eV, account for most, $\sim 70\%$, of the $I_{\mathrm{rel}}(2p_{1/2})$ in this peak; very roughly, these peaks are the analogues in O_h^* of the $J=2$ and $J=3$ levels arising from the coupling of $3d^5(^6S_{5/2})$ with a $2p_{1/2}$ hole. All these features indicate that many-body effects are more important for $2p_{1/2}$ than for $2p_{3/2}$ ionization. The intensities from $2p_{1/2}$ and $2p_{3/2}$ contribute about equally to the satellite intensity in peak 2 at $6 \leqslant E_{\mathrm{rel}} < 9$ eV while the intensity from $2p_{1/2}$ makes the major contribution to the intensity of the satellites in peak 4 at $16 \leqslant E_{\mathrm{rel}} < 22$ eV; see Table IV.

The center of gravity of peak 2 for the $2p$ XPS with the embedded MnO_6 cluster shifts by 0.5 eV from the position for the free Mn^{2+} cation to $E_{\mathrm{rel}}\sim 7$ eV; it is now reasonably close to the position of this satellite in the experimental XPS; see Fig. 3. The energy shift can be understood in terms of the recoupling of the $3d^5$ electrons and their coupling with the open $2p$ shell. We argue by analogy to the nonrelativistic results for the Mn $3p$ hole where the analysis is simpler. In this case, Freeman *et al.*[14] showed that the multiplet responsible for the low-energy satellite of the main peak was dominated by a recoupling of the $3d^5$ electrons to XPS forbidden ^4P and ^4D multiplets with only $\sim 30\%$ of the XPS-allowed ^6S multiplet. The excitation energies to these XPS-forbidden couplings are given by suitable combinations of exchange integrals, $K(3d,3d)$ and $K(2p,3d)$.[57] As shown in Table II for the $2p$-hole orbitals, the $\bar{K}(3d,3d)$ and $\bar{K}(2p,3d)$ for the MnO_6 cluster decrease from the atomic values by $\sim 10\%$ because of the covalent character of the cluster orbitals. This decrease in the exchange integrals is consistent with and explains the decrease in E_{rel} for the MnO_6 cluster model of MnO.

There is a similar shift of ~ 0.6 eV to lower binding energy (BE) for the dominantly $2p_{1/2}$ ionization in peak 3 for the MnO_6 cluster model of MnO compared to the values for the isolated Mn^{2+} cation. Since the many-body effects are more important for the $2p_{1/2}$ peaks than for the $2p_{3/2}$ peaks (see the discussion above), it is difficult to make a detailed analysis that relates the BE shifts to the exchange integrals. However, the reasoning that the reduction of the exchange integrals by $\sim 10\%$ due to the increase in covalent character in the ionic state orbitals of the cluster leads to a shift to lower BE by ~ 0.5 eV should apply to peak 3 as well as to peaks 1 and 2. It should also be noted that the global shape of peak 3 for the MnO_6 cluster has also changed from that for the isolated cation. These changes in the shape arise because of the ligand-field splittings and the reduction of symmetry for the O_h^* double group compared to atomic symmetry. Both the lowering of E_{rel} and the changes in the global shape of the peak have improved agreement with the measured XPS for MnO (Fig. 3). However, there are still noticeable differences between the theoretical and experimental XPS for this peak. Inclusion of new classes of configurations in the DCI WF to represent additional many-body effects should be made to determine if they improve the overall agreement between theory and experiment for this peak. Two classes of configurations should be considered. The first class involves configurations that include excitations from the Mn $3p$ shell into the $3d$ shell. These configurations have been shown to improve the muliplet splittings of the various couplings of the electrons in the $3d$ shell.[67] The second class of configurations are the CT configurations, $d^{n+1}\underline{L}$, where an electron is transferred from the cluster closed-shell orbitals of e_g and t_{2g} symmetries into the open-shell orbitals of these symmetries. Including these CT configurations will enable us to determine if CT into the open-shell space contributes to changes in the details of the energy and shape of the XPS, especially for peak 3.

Finally, we comment briefly on peak 4 at $E_{\mathrm{rel}}\sim 20$ eV, which dominantly arises from many-body satellites of the main $2p_{1/2}$ peak, peak 3; see Table IV. This peak shifts to somewhat lower BE when the MnO_6 cluster model is used; presumably, this is for the same reason as for the shifts for the other peaks. The total intensity going into this peak, relative to that for the other three XPS peaks, is also somewhat reduced, by about 15%, from that obtained with the isolated Mn^{2+} cation. The intensity obtained with the MnO_6 cluster model is not at the correct energy, and it is not of sufficiently high intensity to account for the peak in the observed XPS of MnO. Clearly our materials and many-electron models are not adequate to explain this peak. We raise the question of whether the peak is an intrinsic XPS satellite or whether it may be an extrinsic loss feature. It has been suggested that extrinsic, plasmon losses make a significant contribution to the XPS of MnO and that they lead to loss features at ~ 20 eV from the leading edge of several peaks including $O(1s)$ and $Mn(3s)$.[68] If peak 4 is an intrinsic XPS feature, it may well arise by including CT configurations of the form $d^{n+1}\underline{L}$ into the DCI WF's. If including these CT configurations in *ab initio* DCI WF's for the MnO_6 cluster does not account for the intensity in peak 4, this will be strong evidence that the peak has an extrinsic origin.

The earliest calculations for the $2p$ and $3p$ XPS of Mn^{2+} cations that included relativistic effects were performed by Gupta and Sen.[15] They studied both the isolated cation and the cation in a crystal field adjusted for MnF_2. They constructed and diagonalized a Hamiltonian that included parameters for the atomic two-electron integrals, the atomic spin-orbit splitting, and the crystal-field splitting. Their model contained some, but not all, of the atomic many-body effects included in the present work and in other prior work on Mn;[1,3–5] the atomic many-body terms that they neglected will be discussed further below. However, they used two-electron integrals determined with nonrelativistic orbitals for the ground state of the Mn atom, where the core p shells are filled. As we see from Table II, this means that the average exchange integrals that they used will be too small by $\sim 20\%$. The use by Gupta and Sen[15] of two-electron integrals that are too small is responsible for the fact that they find values of E_{rel} that are modestly smaller than our values for either the Mn^{2+} cation or the embedded MnO_6 cluster. The reduction of the energy splittings is most easily seen for the first XPS peak that arises from the coupling of $2p_{3/2}$ with $3d^5(^6S_{5/2})$.Moreover, for this peak, they computed I_{rel} values

for the $J=3,2$, and 1 levels, relative to the $J=4$ level intensity, that are larger than the values that we report in Table III. This discrepancy is due to the fact that they did not consider all possible angular momentum couplings within the $3d$ shell. Gupta and Sen[15] only included states where the nonrelativistic coupling of the p^5d^5 was to ^7P or ^5P. However, they neglected the levels that, although XPS forbidden, can mix with the XPS-allowed levels and steal intensity from them. This is the reason why, in the Gupta-Sen work, there is too little intensity lost from XPS peak 1 and too little intensity appears in satellite peaks, especially peak 2. While the Gupta-Sen treatment is correct in the nonrelativisitic limit, it is not correct when spin-orbit effects are included.

Later, Yamaguchi *et al.*[20] reported a crystal-field study of the $2p$ and $3p$ XPS of several TM compounds, including MnO. They appear to have included all the appropriate relativistic angular momentum many-body effects[1,3] in their model Hamiltonian. While they use, as did Gupta and Sen,[15] atomic two-electron interaction integrals appropriate for the ground state of Mn without a core hole, they have scaled the two-electron integrals to smaller values by factors of 30%–40%. These scalings are considerably different from those that we find (see Table II), and they are considerably larger than the scalings used by Kotani and collaborators;[4,6] in effect, Yamaguchi *et al.* use two-electron integrals that are much too small. As a result, their predicted Mn $2p$ XPS is quite different from our spectra and from experiment. In particular, it appears that their XPS peak 1 is very broad and their peak 2 has almost merged with peak 1. This compression of XPS peak 2 into peak 1 is entirely consistent with our analysis of the consequences of using very small two-electron integrals.

The np XPS of MnO has also been studied by Kotani and collaborators.[4,6] They solved a semiempirical, parametrized model Hamiltonian; their model takes into account the same intra-atomic many-body effects and relativistic spin-orbit splittings that we have used. However, they also included CT configurations for both one-electron, $d^{n+1}\underline{L}$, and two-electron, $d^{n+2}\underline{L}^2$, transfers from the ligand to the TM open d shell. On the other hand, they did not include covalent mixing of the TM $3d$ orbitals and the ligand $2p$ orbitals; further, they also neglected the overlap of the TM $3d$ orbital with the ligand $2p$ orbital. They use several parameters to describe both intraatomic and inter-atomic effects and, for the most part, the values of these parameters are adjusted to improve the agreement of their calculated XPS spectra with experiment. A matter of particular interest is the importance of $d^{n+1}\underline{L}$ and $d^{n+2}\underline{L}^2$ CT configurations. Kotani and collaborators[4–6] claim that these CT configurations are important. Most recently,[5] they have stated that the CT configurations are particularly important for "the spectral shape of the satellite at about 6 eV"; this is the $2p$ XPS peak that we have labeled peak 2 in Fig. 3. Whereas the MnO_6 model has represented the XPS in the region of peak 2 better than the atom model, there is still significant missing density between the first and second peaks. Thus, although including covalency is necessary, it is not sufficient to fully explain the region around the second peak. This indicates that some key physics is missing from the model, possibly CT. Inclusion of CT configurations in our cluster model is beyond the scope of the present paper.

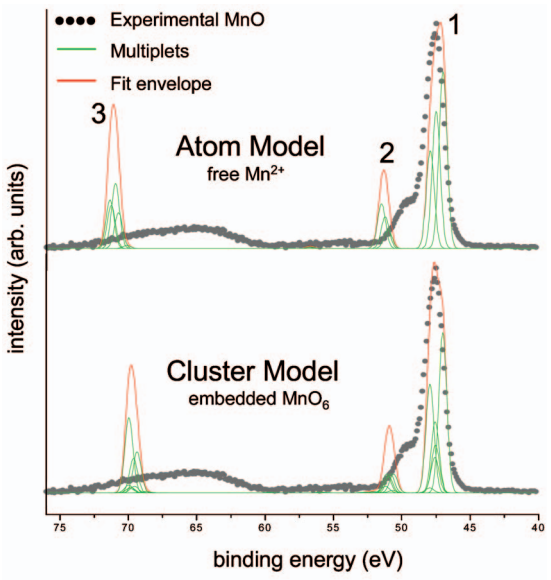

FIG. 4. (Color) $3p$ XPS for Mn^{2+} and for the embedded MnO_6 cluster compared to experiment. For both the atomic and cluster model results, the first calculated multiplet at $E_{rel}=0$ eV has been placed at $E=47.0$ eV to give the best fit to the experimental $3p$ XPS for MnO.

B. Mn $3p$ XPS

The theoretical and experimental Mn $3p$ XPS are shown in Fig. 4. This figure follows the conventions used for Fig. 3, where the Gaussian-broadened contributions of individual ionic levels from the DCI WF's as well as the envelope of the sum of the individual levels are shown. We refer our calculated relative energies E_{rel} to the measured $3p$ XPS energies with an energy scale where $E_{rel}=0$ is placed at 47.0 eV. Three regions are of interest for the Mn $3p$ XPS. The first, lowest BE peak has a full width at half maximum (FWHM) of ~1.5 eV, and $E_{rel}=0$ is the position of the first theoretical XPS peak. The second feature is a shoulder in the measured XPS at $E_{rel}\approx 3.0$ eV, and the third feature is a very broad peak, about 20 eV wide, centered at $E_{rel}\approx 20$ eV. The theoretical results for the second peak, or shoulder, give a separate peak at $E_{rel}\sim 4$ eV—i.e., at somewhat too high a BE. The theoretical results for the third feature give a fairly narrow peak at $E_{rel}\sim 23$ eV; the levels contributing to this peak, for both Mn^{2+} and MnO_6, cover a range of only ~0.5 eV. The width of the peak is not at all consistent with experiment.

As seen from Fig. 4, the first XPS peak is very similar for both the Mn^{2+} and MnO_6 models. Indeed, the theoretical peak for MnO_6 is even slightly broadened, by ~0.05 eV. This appears to contradict our previous analysis that the covalency included in the MnO_6 cluster model produces a small narrowing, ~0.4 eV, of the leading peak in the Mn $2p$ XPS. At first sight, one would expect that a similar narrowing would occur for the Mn $3p$ XPS; however, this expectation does not take into account the different coupling of the $3p$ hole with the $3d^5(^6S_{5/2})$ shell. For the first Mn $2p$ XPS peak, we showed that the coupling was of the open $2p_{3/2}$ shell with $3d^5$-coupled $^6S_{5/2}$ and that the different J levels

TABLE V. The individual $3p$-hole levels in the first Mn($3p$) XPS peak for Mn^{2+} and for an embedded MnO_6 cluster model of MnO. The levels are grouped according to their J value. For Mn^{2+}, J is a good quantum number and the states with a given J are exactly degenerate; for MnO_6, J is only an approximate quantum number and the degeneracy of the J states is lifted. The states with different energies are listed separately; however, when the states are within 0.02 eV, they are grouped together. The number of states for a given E_{rel}, in eV, and the SA I_{rel} for these states are given; for MnO_6, the total I_{rel} for the states associated with a J value is also given. Further for MnO_6, the numbers of $3p_{1/2}$ and $3p_{3/2}$ electrons, $n(3p_{1/2})$ and $n(3p_{3/2})$, in the DCI WF's are given.

	Mn(2+)			MnO_6				
J	E_{rel}	No. of states	I_{rel}	E_{rel}	No. of states	I_{rel}	$n(3p_{1/2})$	$n(3p_{3/2})$
4	0	9	9	0.00–0.02	5	5	1.99	3.01
				0.05	2	2.00	1.99	3.01
				0.10	2	2.00	2.00	3.00
					Sum	9.00		
3	0.51	7	6.98	0.49	2	1.99	1.64	3.36
				0.54	2	1.99	1.64	3.36
				0.58–0.59	3	2.99	1.63	3.37
					Sum	6.97		
2	0.93	5	4.98	0.95–0.96	3	2.99	1.30	3.70
				0.98	2	1.99	1.30	3.70
					Sum	4.98		

that arose from this coupling were split by the exchange integrals between the $2p$ and $3d$ shells. For the Mn $3p$ XPS, it is more appropriate to consider the first peak as arising from a Russell-Saunders multiplet of ^7P, or in O_h of $^7T_{1u}$, symmetry, which is then split by the spin-orbit coupling of the total $S=3$ and $L=1$ into $J=4$, 3, and 2 levels.[1,14] The different coupling is due to the much smaller spin-orbit splitting for the $3p$ shell than for the $2p$ shell.[57,62] The spin-orbit splitting of this Russell-Saunders multiplet is given by the Landé interval rule, and the driving force is the one-electron matrix element giving the spin-orbit coupling in the $3p$ shell.[42,57,62] Since the $3p$ orbital is essentially a core orbital and is not changed greatly by the environment of the Mn^{2+} cation, the spin-orbit splitting should not change significantly between that for the isolated cation and for the embedded cluster model of MnO.

We give in Table V a detailed comparison of the E_{rel} and SA I_{rel} for the individual levels and states that contribute to the Mn $3p$ XPS for Mn^{2+} and MnO_6 materials models. The levels are grouped according to the J value with which they are associated. Since J is a good quantum number, for the isolated atom, the states in a given J level are exactly degenerate; for the O_h^* double group of MnO_6, J is only an approximate quantum number and the states are split by ligand- and crystal-field effects.[42] As we discuss below, this splitting is much larger than for the $2p$-shell levels. For MnO_6, we separate these crystal-field splittings and give E_{rel} for degenerate states or for states spaced very closely, within 0.02 eV. For these groups of states, we give the number of states included in the group. For the lowest-energy states, $E_{rel}=0$. The SA I_{rel} are scaled so that the value for the lowest-energy group is the number of states contained in that group; thus, $I_{rel}=9$ for the $J=4$ level of Mn^{2+} and $I_{rel}=5$ for the five states of the MnO_6 cluster with $0 \leqslant E_{rel} < 0.02$ eV. This normalization of I_{rel} has been chosen so that we can examine the differential importance of the many-body and relativistic effects included in the DCI WF's and of the effect of using different orbitals for the initial and final states. The latter concern is for whether what we have called closed-shell screening[2] is more important for some of the $3p$-hole states than for other $3p$-hole states. If these effects are equally important for all the hole states, then with our chosen normalization all the I_{rel} should be equal to the integer number of states contained in the individual groups.[29,61] The near-integer values of I_{rel} in Table V clearly show that there are no significant differential effects for the states in the first XPS peak for either the Mn^{2+} or MnO_6 models of MnO. The spin-orbit splittings for both models are quite similar. It appears that the splittings are modestly larger for the MnO_6 cluster than for the isolated Mn^{2+} cation but this is because the ligand-field splittings in the MnO_6 levels raise the average energy of the nine lowest states from $E_{rel}=0$ to $E_{rel}=0.04$ eV. The average energies of the ligand-field-split MnO_6 states for each of the J levels give spin-orbit splittings that are essentially the same as for Mn^{2+}.

These spin-orbit splittings can be easily understood by examining the numbers of $3p_{1/2}$ and $3p_{3/2}$ electrons contained in the MnO_6 DCI WF's; in the O_h^* double group, these are the numbers of electrons in the $3p$ spinors of γ_{6u} and γ_{8u} symmetries, respectively. When nearly degenerate states are included in a group, the $n(3p_{1/2})$ and $n(3p_{3/2})$ are averaged for the different states but this averaging does not lead to important changes. These occupations are essentially the same for all the states associated with a given J level, and they are also very nearly the same as the occupations determined for the states of the isolated Mn^{2+} cation. This is further evidence that the $3p$-hole states determined for the cation and cluster are very similar. The $3p$ hole for $J=4$ is essentially a pure $p_{3/2}$ hole with $n(3p_{3/2})=3$, one less than the closed-shell occupation of 4. This is because, as explained above for the $2p$-hole states, only $j=3/2$ can couple with the $J=5/2$ of $d^5(^6S_{5/2})$ to give a total $J=4$. However, the $J=3$ states have 0.6 of a $3p_{3/2}$ hole and 0.4 of a $3p_{1/2}$ hole and the $J=2$ states have 0.3 of a $3p_{3/2}$ hole and 0.7 of a $3p_{1/2}$ hole. These excitations are needed to represent the L-S coupling of the Russell-Saunders multiplet in terms of determinants formed with the spinors.[62] A good estimate of the energy to change a $3p_{3/2}$ hole into a $3p_{1/2}$ hole is given by the difference of the orbital energies for the spin-orbit split spinors, $\Delta\varepsilon(3p_{3/2}\text{-}3p_{1/2})$. For the cation, $\Delta\varepsilon(3p_{3/2}\text{-}3p_{1/2})=1.39$ eV, and for MnO_6, the value is very similar, $\Delta\varepsilon(3p_{3/2}\text{-}3p_{1/2})=1.36$ eV. The spin-orbit splitting of the ^7P multiplet is estimated by multiplying $\Delta\varepsilon(3p_{3/2}\text{-}3p_{1/2})$ by the fraction of a hole changed; this gives a ΔE for $J=3$ of 0.5 eV and for $J=2$ of 1.0 eV, in good agreement with the directly calculated values. The small difference of the $3p$ spin-orbit splittings between Mn^{2+} and MnO_6 is a major reason that the MnO_6 $3p$ XPS is very similar to the $3p$ XPS for the isolated Mn^{2+}

cation. The additional splittings introduced in the $3d$ orbitals in O_h^* also help to explain the energy splittings of the MnO_6 "J levels." The fourfold-degenerate e_g d orbitals in O_h are not split further and go into fourfold-degenerate γ_{8g} spinors in O_h^*. However, the sixfold-degenerate t_{2g} orbitals split into twofold-degenerate γ_{7g} and fourfold degenerate γ_{8g} spinors in O_h^*. The splitting of these two spinors is 0.07 eV, comparable to the 0.03–0.10 eV range of energy splittings for the MnO_6 states associated with a given J level.

The use of spinors optimized for the $3p$-hole state of MnO_6 and the resulting increase in covalency and closed-shell screening of the $3p$ hole (see Table I) lead to a modest loss of intensity in this first $3p$ XPS peak. There is a 14% loss in I_{rel} from the intensity that would have been obtained if the same orbitals had been used for both the initial- and $3p$-hole-state configurations. The other peaks also have similar losses, and these losses are not recovered in the states included in our complete open-shell DCI calculations. As for the $2p$-hole states, this intensity is likely to go to relatively high-energy shake states. However, it will be valuable to examine how much of this intensity will be recovered when CT configurations are included in the DCI.

The second peak in the calculated $3p$ XPS for Mn^{2+} consists of intensity from states with $4.0 \leqslant E_{\mathrm{rel}} \leqslant 4.5$ eV, which have an intensity that is 23% of the intensity in the first peak; see also Ref. 1. These states have been assigned as arising from low-spin-coupled ^5P, $^5T_{1u}$, states that have a major, ~70%, contribution from the XPS-forbidden states where the d^5 shell is recoupled away from the allowed ^6S coupling.[1,14] When closed-shell screening is taken into account with the MnO_6-embedded cluster model of MnO, the second $3p$ XPS peak moves to a lower-energy range of $3.6 \leqslant E_{\mathrm{rel}} \leqslant 4.10$ eV with 21% of the intensity of the first peak. While the intensity in the peak is not significantly changed from the value for the isolated Mn^{2+} cation, the peak shifts to 0.4 eV lower BE; this 10% decrease in E_{rel} is the same as the decreases for the $2p$ XPS (see above). The excitation energies to the diagonal matrix elements of the configurations involved in this excitation involve exchange integrals for the $3d$-$3d$ and $3p$-$3d$ interactions.[57] As shown in Table II, the average exchange integrals $\bar{K}(3d,3d)$ and $\bar{K}(3p,3d)$ are reduced by 6% and 8%, respectively, from the values for the isolated Mn^{2+} cation. This decrease in the exchange integrals leads, in turn, to a decrease in the excitation energies and, hence, in the E_{rel} of higher-BE peaks. The magnitude of the decrease of the $\bar{K}$ is consistent with the magnitude of the decrease in E_{rel}. Further, we have shown that this decrease in $\bar{K}$ is due to the covalent mixing of metal $3d$ and ligand $2p$ orbitals, which is more important in the orbitals optimized for the final, ionic states because it allows for increased closed-shell screening of the metal core hole. The E_{rel} for this second peak is still too large by ~1 eV but this is most likely due to our neglect, as discussed previously for the Mn $2p$-hole XPS, of the many-body effects needed to correctly describe the splittings of the various $3d^5$ angular momentum couplings.[67]

The third peak in the calculated $3p$ XPS for Mn^{2+} arises primarily from states with $23.7 \leqslant E_{\mathrm{rel}} \leqslant 24.4$ eV; these states have an intensity that is 47% of the intensity in the first peak. They have been assigned to low-spin-coupled ^5P, $^5T_{1u}$, states that have a dominant, ~65%, contribution from states where the d^5 shell is coupled to ^6S.[1,14] For the MnO_6 cluster model, this XPS peak moves to a lower energy range of $22.4 \leqslant E_{\mathrm{rel}} \leqslant 23.0$ eV, still with 47% of the intensity of the first peak. The main change is that the BE of the peak is lowered by 1.4 eV or by 6% due to covalency and closed-shell screening of the core hole, which decreases the exchange integrals. While this reduction in E_{rel} brings the position of the calculated peak into slightly better agreement with experiment, we still fail to explain the very large width of the observed peak. Indeed, the energy width of the calculated levels with intensity in this region has not changed between the isolated cation and the embedded MnO_6 cluster. This negative result for the width of the XPS peak at E_{rel} ~20 eV leads us to consider below the suggestion made by Taguchi *et al.*[4] that the peak is broadened by corehole lifetime effects.

Hermsmeier *et al.*[30] showed that the Mn $3p$ XPS for Mn (gas), MnF_2, and MnO are similar; they concluded that atomic effects dominate for the Mn XPS. Our analysis supports their interpretation and provides a quantitative understanding of differences and similarities between the XPS for the isolated atom and for MnO; we apply this analysis to examine aspects of the data in Hermsmeier *et al.*[30] The first XPS peak appears to have a very similar FWHM for Mn gas, MnF_2, and MnO, consistent, as we argued above, with the origin of this peak as a spin-orbit-split Russell-Saunders ^7P, multiplet. If the small broadening of this peak for MnO_6 over that for Mn^{2+}, which we have ascribed to additional splittings in the O_h^* double group, were also found in their MnF_2 and MnO spectra, this would lend strong support to our analysis. For Mn gas, peak 2 is a separate peak at 3.1 eV from the main peak, while from our calculations for isolated Mn^{2+}, the separation of the centers of peaks 1 and 2 is $\Delta E = 3.9$ eV. As we explained above, our ΔE is too large because we have not correctly described the separations of the $3d^5$ muliplet couplings to ^6S, ^4P, and ^4P. However, Hermsmeier *et al.*[30] find that this ΔE becomes smaller for the compounds; it remains a separate peak for MnF_2 but it is only a shoulder on peak 1 for MnO. We have shown that ΔE is reduced from the cation to MnO because the covalent character of the d orbitals leads to a smaller exchange integral, $K(3p,3d)$; see Table II. It is believed that MnF_2 is a more ionic system than MnO; hence, there will be less covalency in MnF_2 and $K(3p,3d)$ will be larger than for MnO. This is consistent with the change in the separation of peaks 1 and 2 between MnF_2 and MnO.

The position of the peak at ~17 eV, which we label as peak 3, does not shift noticeably from the XPS for Mn gas to either MnF_2 or MnO; however, this peak for MnF_2 broadens somewhat from Mn gas and for MnO it broadens considerably. Taguchi *et al.*[4] have ascribed the broadening of peak 3 to lifetime broadening of the XPS final states, which they assume will have a linear dependence on the energy of a state relative to the lowest energy $3p$-hole state. With a suitable chosen parameter for the energy dependence of the lifetime broadening, they are able to reproduce the observed extremely broad peak 3. However, based on their arguments, one would predict an even broader peak 3 for Mn gas. We have shown that the position of this third peak is at a slightly

larger ΔE for the Mn atom than for MnO by $\sim$1.4 eV, or $\sim$5%, and Taguchi *et al.*[4] assume that the broadening increases with increasing ΔE. This conclusion is opposite to the XPS data of Hermsmeier *et al.*,[30] who find a dramatically narrower peak 3 for Mn gas. Thus the assumed energy-dependent lifetime broadening does not provide a consistent explanation of the very different broadenings of this peak between Mn gas and MnO.

We compare our results for the Mn $3p$ XPS with those reported by Gupta and Sen.[15] As discussed in Sec. IV A, Gupta and Sen did not include all of the Russell-Saunders couplings of the p^5d^5 in their effective Hamiltonian for either the $2p$ or $3p$ XPS. This omission is less important for the $3p$ XPS since spin-orbit splitting of the $3p$ shell is almost an order of magnitude smaller than for the $2p$ shell and the treatment of Gupta and Sen is correct in the limit that spin-orbit splitting is neglected. There are other small differences due to their choice of the two-electron interaction integrals using atomic values and their choice of crystal-field parameters for MnF_2 rather than MnO. Overall, the differences of their results and our results with the MnO_6 cluster are not especially large for the Mn $3p$ XPS. On the other hand, the crystal-field results of Yamaguchi *et al.*[20] are very different from our *ab initio* results for either Mn^{2+} or MnO_6. There is a considerable compression of the features reported by Yamaguchi *et al.* compared to our results, and this compression is due to the very large reduction factors of 30%–40% that they used to scale the atomic values for the two-electron interaction integrals. As well as this compression of energy differences, the individual peaks that they report are substantially broadened over our results; this broadening may be due to the fact that they used a very large $10D_q$=4.0 eV to represent crystal-field splittings. Finally, we comment only briefly on the results of Taguchi *et al.*[4] for the Mn $3p$ spectra since relevant issues have been raised concerning their results previously in this section. Their results are reasonably close to experiment, especially after they introduce an *ad hoc* energy-dependent lifetime broadening to explain the high-energy XPS peak. However, we point out they find, as we do, that peak 2 at $\sim$3 eV, relative to the main peak, is a separate peak rather than the shoulder observed in the XPS measurements. Their model Hamiltonian does not contain the electron correlation effects required to give the correct splittings for the different multiplets of the $3d^5$ configuration. The fact that such electron correlation effects are not taken into account in their model Hamiltonian is one of the reasons given to justify the scaling of the two-electron interaction integrals to smaller values.[18] However, the fact that Taguchi *et al.*[4] still incorrectly predict a distinct XPS peak for peak 2 of the Mn $3p$ XPS suggests that scaling exchange integrals to reduce them from their atomic values are not sufficient to correctly reproduce atomic multiplet splittings. It may well be, as we have argued, that the scaling is necessary to include the effects of covalency that reduces the exchange integrals from their atomic values.

V. CONCLUSIONS

We have presented a detailed analysis of the physical origins of environmental, interatomic, effects on the Mn $2p$ and $3p$ XPS of MnO. Our theoretical model is based on *ab initio* fully relativistic WF's for an embedded MnO_6 cluster model of MnO. The relaxation and screening of the core hole is taken into account by optimizing the spinors for the core-hole configurations as well as for the initial-state configuration where the core hole is absent. The mutual nonorthogonality of the sets of spinors used for the initial- and final-state configurations has been correctly included in the calculation of the SA I_{rel} for the XPS. This exact calculation of the SA I_{rel} represents a major advance over prior work that includes spin-orbit coupling. Prior *ab initio* atomic DCI calculations[1,3] neglected the nonorthogonality of the initial and final-state spinors. For atoms, this is acceptable because the radial contractions of atomic orbitals in the presence of a core hole do not lead to large deviations from orthogonality between the orbital sets. However, for cluster representations of the condensed phase, the change in covalency of the spinors for the different configurations leads to much larger deviations from orthogonality and must be taken into account. Furthermore, semiempirical models for TM XPS assume a common orbital set for both initial and core-hole states and, in addition, assume that the orbitals are either pure TM or pure ligand and do not have covalent mixing of these atomic characters. We have shown that these assumptions have consequences for the energy spacing and for the width of features in the XPS spectra.

Our WF's included many-body effects for the intra-atomic terms that represent angular momentum coupling and recoupling within the d shell and between the d and core-hole p shells. For the interatomic effects, we only included the one-electron terms represented by covalency and by ligand-field splitting of the d orbitals in the O_h^* double group. We have not included the many-body interatomic effects represented by $d^{n+1}\underline{L}$ CT configurations. The CT configurations were not included so that we could specifically and systematically investigate the consequences of the interatomic one-electron effects to modify the intra-atomic many-body effects in the ligand environment. We were able to show that including covalency had a significant effect on the calculated Mn $2p$ spectrum for MnO, where, in general, covalency aligned the calculations closer to experiment. Further, we were able to quantify the contributions of one-electron interatomic effects, which were included in our *ab initio* cluster model. Finally, our analysis allowed us to identify the remaining open questions for the origin of certain XPS features.

We have shown that there is a differential covalency between the core-hole and initial-state configurations. For MnO, the increased covalency when the core hole is present leads to an increase of $\sim$0.3 d electrons, which helps to screen the core hole. Since this increase occurs in the closed-shell orbitals that have dominantly ligand character, it is appropriate to describe this as closed-shell screening, an effect that has not been directly included in semiempirical XPS models. We have shown that the delocalization of the dominantly TM $3d$, open-shell orbitals leads to a decrease of the exchange integrals that are involved in the multiplet splittings. In general, we have been able to relate the decrease in the exchange integrals to a decrease in the width of individual features and to decreases in the energetic separations between these features. We have also been able to explain

when and why this general decrease will not hold. Thus, the first peak in the Mn $2p$ XPS is narrowed because the splitting of the J levels contained in this peak is largely determined by the $K(2p,3d)$ exchange integral. On the other hand, the first peak in the Mn $3p$ XPS is not narrowed because the splitting of the J levels contained in this peak depends on the $3p$ spin-orbit splitting and not on $K(3p,3d)$. The slight broadening of this peak has been related to the additional splittings in O_h^* compared to the nonrelativistic O_h point group.

The magnitude of the energy narrowings and shifts going from Mn^{2+} to MnO is $\sim$0.5 eV. However, closed-shell screening, while modest for MnO, is larger[2] by a factor of $\sim$2.5 for Cr_2O_3. Thus, covalency may lead to even larger decreases of energy spacings in other TM ionic materials. Our work shows that a scaling of the atomic values of the exchange integrals is required to account for the covalency of the open-shell orbitals in the compounds. This reason has not been given to justify the scaling used in semiempirical approaches. Furthermore, the fact that the covalency is different for t_{2g} and e_g orbitals suggests that it may be necessary to use different scaling factors for the exchange integrals over orbitals with these symmetries. Unfortunately adjusting the values of additional parameters may further mask the physics that relates the XPS to the electronic structure of the materials.

We have also analyzed the Mn XPS calculations reported by Gupta and Sen[15] and by Yamaguchi *et al.*[20] We have shown that Gupta and Sen omitted certain intra-atomic many-body effects that are especially important for the $2p$ XPS; these many-body effects were also omitted from their XPS calculations for other TM cations.[16] Since their results are regularly used to determine TM oxidation states from measured XPS, it is important to be aware of this limitation. For the work of Yamaguchi *et al.*,[20] we have shown that the very large factors that they used to scale the two-electron interaction integrals lead to major changes in XPS features that are not consistent with experimental data.

Our analysis has raised certain questions about the interpretation of the Mn XPS. For the $2p$ XPS, the intensity in the highest BE peak, peak 4 in Fig. 3, decreases for the MnO_6-embedded cluster compared to the intensity for the isolated Mn^{2+} cation; the MnO_6 results do not appear to account for the measured intensity. Hence, we ask whether peak 4 is an intrinsic feature of the XPS due to many-electron effects not included in our DCI or if it is an extrinsic feature caused, for example, by plasmon losses. Also, covalency does not account for the intensity between the first and second peak. This missing intensity may reflect a need to include CT configurations such as $d^{n+1}\underline{L}$. For the $3p$ XPS, the MnO_6 cluster results do not significantly broaden the highest-BE peak at $E_{\mathrm{rel}}=\sim 20$ eV over the results for the isolated Mn^{2+}. This peak is $\sim$10–15 eV wide and has been ascribed to lifetime effects for the $3p$-hole states. We have pointed out that the lifetime effects that have been invoked do not appear to be consistent with the much narrower width of this peak measured for atomic Mn. We ask if many-body effects associated with CT configurations could account for this very broad peak. In particular, the coupling of charge transfer excitations with the use of covalent orbitals for the dominantly ligand closed shells and for the dominantly TM d open shells might distinguish the Mn atom from MnF_2 and MnO. Further insight into these open questions will be gained from relativistic and nonrelativistic cluster model WF's where covalency and charge transfer are treated on an equal footing.

ACKNOWLEDGMENTS

This research was supported, in part, by the Geosciences Research Program, Office of Basic Energy Sciences, U.S. Department of Energy (DOE). A portion of the research was performed at the W. R. Wiley Environmental Molecular Sciences Laboratory, a national scientific user facility sponsored by the U.S. DOE and located at PNNL, operated for the DOE by Battelle. We are also pleased to acknowledge partial computer support from the National Center for Supercomputing Applications, Urbana-Champaign, Illinois. One of us (P.S.B.) acknowledges partial support from the National Science Foundation under Grant No. NSF CHE03-4999. Finally, we wish to thank L. Sangaletti for providing us with digital files of the XPS data for MnO that facilitated our comparisons of theoretical with experimental spectra.

[1] P. S. Bagus, R. Broer, W. A. de Jong, W. C. Nieuwpoort, F. Parmigiani, and L. Sangaletti, Phys. Rev. Lett. **84**, 2259 (2000).
[2] P. S. Bagus, E. S. Ilton, and J. R. Rustad, Phys. Rev. B **69**, 205112 (2004).
[3] E. S. Ilton, W. A. deJong, and P. S. Bagus, Phys. Rev. B **68**, 125106 (2003).
[4] M. Taguchi, T. Uozumi, and A. Kotani, J. Phys. Soc. Jpn. **66**, 247 (1997).
[5] M. Taguchi, T. Uozumi, K. Okada, H. Ogasawara, and A. Kotani, Phys. Rev. Lett. **86**, 3692 (2001).
[6] K. Okada and A. Kotani, J. Phys. Soc. Jpn. **61**, 4619 (1992).
[7] P. S. Bagus, R. Broer, C. de Graaf, and W. C. Nieuwpoort, J. Electron Spectrosc. Relat. Phenom. **99**, 303 (1999).
[8] A. H. de Vries, L. Hozoi, R. Broer, and P. S. Bagus, Phys. Rev. B **66**, 035108 (2002).
[9] C. deGraaf, R. Broer, W. C. Nieuwpoort, and P. S. Bagus, Chem. Phys. Lett. **272**, 341 (1997).
[10] B. Hermsmeier, C. S. Fadley, M. O. Krause, J. Jimenez-Mier, P. Gerard, and S. T. Manson, Phys. Rev. Lett. **61**, 2592 (1988).
[11] B. W. Veal and A. P. Paulikas, Phys. Rev. Lett. **51**, 1995 (1983).
[12] B. W. Veal and A. P. Paulikas, Phys. Rev. B **31**, 5399 (1985).
[13] P. S. Bagus, R. Broer, and E. S. Ilton, Chem. Phys. Lett. **394**, 150 (2004).
[14] A. J. Freeman, P. S. Bagus, and J. V. Mallow, Int. J. Magn. **4**, 35 (1973).
[15] R. P. Gupta and S. K. Sen, Phys. Rev. B **10**, 71 (1974).
[16] R. P. Gupta and S. K. Sen, Phys. Rev. B **12**, 15 (1975).
[17] P. S. Bagus, H. J. Freund, T. Minerva, G. Pacchioni, and F.

Parmigiani, Chem. Phys. Lett. **251**, 90 (1996).
[18] F. M. F. deGroot, J. Electron Spectrosc. Relat. Phenom. **67**, 529 (1994).
[19] P. A. Cox, *Transition Metal Oxides: An Introduction to their Electronic Structure and Properties* (Clarendon Press, Oxford, 1992).
[20] T. Yamaguchi, S. Shibuya, and S. Sugano, J. Phys. C **15**, 2625 (1982).
[21] P. S. Bagus, R. Broer, W. A. de Jong, W. C. Nieuwpoort, F. Parmigiani, and L. Sangaletti, Phys. Rev. Lett. **86**, 3693 (2001).
[22] P. S. Bagus, G. Pacchioni, and F. Parmigiani, Chem. Phys. Lett. **207**, 569 (1993).
[23] F. Parmigiani, G. Pacchioni, F. Illas, and P. S. Bagus, J. Electron Spectrosc. Relat. Phenom. **59**, 255 (1992).
[24] R. A. Phillips and F. P. Larkins, Aust. J. Chem. **39**, 717 (1986).
[25] T. E. Meehan, J. McColl, and F. P. Larkins, J. Electron Spectrosc. Relat. Phenom. **73**, 283 (1995).
[26] P. C. Ford, I. H. Hillier, S. A. Pope, and M. F. Guest, Chem. Phys. Lett. **102**, 555 (1983).
[27] S. Hovel, C. Kolczewski, M. Wuhn, J. Albers, K. Weiss, V. Staemmler, and C. Woll, J. Chem. Phys. **112**, 3909 (2000).
[28] T. Åberg, Phys. Rev. **156**, 35 (1967).
[29] P. S. Bagus, M. Schrenk, D. W. Davis, and D. A. Shirley, Phys. Rev. A **9**, 1090 (1974).
[30] B. D. Hermsmeier, C. S. Fadley, B. Sinkovic, M. O. Krause, J. Jimenez-Mier, P. Gerard, T. A. Carlson, S. T. Manson, and S. K. Bhattacharya, Phys. Rev. B **48**, 12425 (1993).
[31] H. W. Nesbitt and I. J. Muir, Geochim. Cosmochim. Acta **58**, 4667 (1994).
[32] A. R. Pratt, I. J. Muir, and H. W. Nesbitt, Geochim. Cosmochim. Acta **58**, 827 (1994).
[33] H. W. Nesbitt and D. Banerjee, Am. Mineral. **83**, 305 (1998).
[34] D. Banerjee and H. W. Nesbitt, Geochim. Cosmochim. Acta **63**, 3025 (1999).
[35] D. Banerjee and H. W. Nesbitt, Geochim. Cosmochim. Acta **63**, 1671 (1999).
[36] N. S. McIntyre and D. G. Zetaruk, J. Vac. Sci. Technol. **14**, 181 (1977).
[37] N. S. McIntyre and D. G. Zetaruk, Anal. Chem. **49**, 1521 (1977).
[38] A. R. Pratt and N. S. McIntyre, Surf. Interface Anal. **24**, 529 (1996).
[39] R. M. Weaver, J. M. F. Hochella, and E. S. Ilton, Geochim. Cosmochim. Acta **66**, 4119 (2002).
[40] R. W. G. Wyckoff, *Crystal Structures* (Wiley, New York, 1963).
[41] P. S. Bagus, F. Illas, C. Sousa, and G. Pacchioni, in *Electronic Properties of Solids Using Cluster Methods*, edited by T. A. Kaplan and S. D. Mahanti (Plenum, New York, 1995), p. 93.
[42] J. S. Griffith, *The Theory of Transition-Metal Ions* (Cambridge University Press, Cambridge, England, 1971).
[43] L. Visscher, O. Visser, P. J. C. Aerts, H. Merenga, and W. C. Nieuwpoort, Comput. Phys. Commun. **81**, 120 (1994).
[44] T. Saue, V. Bakken, T. Enevoldsen, T. Helgaker, H. J. A. Jensen, J. K. Laerdahl, K. Ruud, J. Thyssen, and L. Visscher, DIRAC, a relativistic *ab initio* electronic structure program, release 3.2, 2000.
[45] P. S. Bagus, B. Liu, A. D. McLean, and M. Yoshimine, CLIPS, a program system to compute *ab initio* SCF and correlated wave functions for polyatomic systems. It has been developed based on the publicly available programs in the ALCHEMY package from the IBM San Jose Research Laboratory.
[46] P. O. Löwdin, Phys. Rev. **97**, 1474 (1955).
[47] F. Prosser and S. Hagstrom, Int. J. Quantum Chem. **2**, 89 (1968).
[48] F. Prosser and S. Hagstrom, J. Chem. Phys. **48**, 4807 (1968).
[49] A. Szabo and N. S. Ostlund, *Modern Quantum Chemistry* (MacMillan, New York, 1982).
[50] A. D. McLean, M. Yoshimine, B. H. Lengsfield, P. S. Bagus, and B. Liu, in *Modern Techniques in Computational Chemistry: MOTECC-90*, edited by E. Clementi (ESCOM Science, Leidon, 1990), p. 593.
[51] L. Sangaletti, L. E. Depero, P. S. Bagus, and F. Parmigiani, Chem. Phys. Lett. **245**, 463 (1995).
[52] C. J. Nelin, P. S. Bagus, and M. R. Philpott, J. Chem. Phys. **87**, 2170 (1987).
[53] C. W. Bauschlicher, Jr. and P. S. Bagus, J. Chem. Phys. **81**, 5889 (1985).
[54] P. S. Bagus, V. Staemmler, and C. Woll, Phys. Rev. Lett. **89**, 096104 (2002).
[55] I. G. Kim, J. I. Lee, and A. J. Freeman, Phys. Rev. B **66**, 174512 (2002).
[56] S. Blaineau and P. Jund, Phys. Rev. B **70**, 184210 (2004).
[57] J. C. Slater, *Quantum Theory of Atomic Structure* (McGraw-Hill, New York, 1960), Vols. I and II.
[58] C. C. J. Roothaan, Rev. Mod. Phys. **23**, 69 (1951).
[59] C. C. J. Roothaan, Rev. Mod. Phys. **32**, 179 (1960).
[60] J. C. Slater, Phys. Rev. **36**, 57 (1930).
[61] L. Sangaletti, F. Parmigiani, and P. S. Bagus, Phys. Rev. B **66**, 115106 (2002).
[62] E. U. Condon and G. H. Shortly, *The Theory of Atomic Spectra* (Cambridge University Press, Cambridge, England, 1951).
[63] E. S. Ilton and P. S. Bagus, Phys. Rev. B **71**, 195121 (2005).
[64] R. Manne and T. Åberg, Chem. Phys. Lett. **7**, 282 (1970).
[65] P. S. Bagus, D. Coolbaugh, S. P. Kowalczyk, G. Pacchioni, and F. Parmigiani, J. Electron Spectrosc. Relat. Phenom. **51**, 69 (1990).
[66] H. J. Freund and E. W. Plummer, Phys. Rev. B **23**, 4859 (1981).
[67] K. Pierloot, E. Tsokos, and B. O. Roos, Chem. Phys. Lett. **214**, 583 (1993).
[68] L. Sangaletti, P. S. Bagus, and F. Parmigiani, Phys. Rev. B **62**, R7695 (2000).